

# Current-limiting amplifier for high speed measurement of resistive switching data

Cite as: Rev. Sci. Instrum. **92**, 054701 (2021); <https://doi.org/10.1063/5.0047571>

Submitted: 15 February 2021 . Accepted: 10 April 2021 . Published Online: 03 May 2021

 T. Hennen,  E. Wichmann, A. Elias, et al.



View Online



Export Citation



CrossMark

## ARTICLES YOU MAY BE INTERESTED IN

[Design and operation of a transportable  \$^{87}\text{Rb}\$  atomic fountain clock](#)



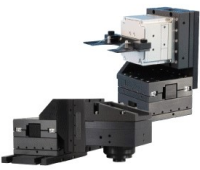
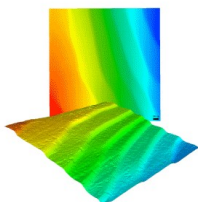
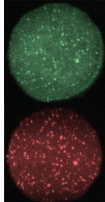
Review of Scientific Instruments **92**, 054702 (2021); <https://doi.org/10.1063/5.0047715>

[Exploiting the switching dynamics of  \$\text{HfO}\_2\$ -based ReRAM devices for reliable analog memristive behavior](#)

APL Materials **7**, 091105 (2019); <https://doi.org/10.1063/1.5108654>

[Cell-phone camera Raman spectrometer](#)

Review of Scientific Instruments **92**, 054101 (2021); <https://doi.org/10.1063/5.0046281>

 <b>MCL</b> MAD CITY LABS INC. <a href="http://www.madcitylabs.com">www.madcitylabs.com</a>	<p>Nanopositioning Systems</p> 	<p>Modular Motion Control</p> 	<p>AFM and NSOM Instruments</p> 	<p>Single Molecule Microscopes</p> 
---	--	--	---	--

# Current-limiting amplifier for high speed measurement of resistive switching data

Cite as: Rev. Sci. Instrum. 92, 054701 (2021); doi: 10.1063/5.0047571

Submitted: 15 February 2021 • Accepted: 10 April 2021 •

Published Online: 3 May 2021



T. Hennen,<sup>1</sup>  E. Wichmann,<sup>1</sup>  A. Elias,<sup>2</sup> J. Lille,<sup>2</sup> O. Mosendz,<sup>2</sup> R. Waser,<sup>1</sup>  D. J. Wouters,<sup>1</sup>   
and D. Bedau<sup>2,a)</sup> 

## AFFILIATIONS

<sup>1</sup>IWE II, RWTH Aachen University, 52074 Aachen, Germany

<sup>2</sup>Western Digital San Jose Research Center, 5601 Great Oaks Pkwy, San Jose, California 95119, USA

<sup>a)</sup> Author to whom correspondence should be addressed: [daniel.bedau@wdc.com](mailto:daniel.bedau@wdc.com)

## ABSTRACT

Resistive switching devices, important for emerging memory and neuromorphic applications, face significant challenges related to the control of delicate filamentary states in the oxide material. As a device switches, its rapid conductivity change is involved in a positive feedback process that would lead to runaway destruction of the cell without current, voltage, or energy limitation. Typically, cells are directly patterned on MOS transistors to limit the current, but this approach is very restrictive as the necessary integration limits the materials available as well as the fabrication cycle time. In this article, we propose an external circuit to cycle resistive memory cells, capturing the full transfer curves while driving the cells in a way that suppresses runaway transitions. Using this circuit, we demonstrate the acquisition of  $10^5$   $I$ ,  $V$  loops per second without using on-wafer current limiting transistors. This setup brings voltage sweeping measurements to a relevant timescale for applications and enables many new experimental possibilities for device evaluation in a statistical context.

Published under license by AIP Publishing. <https://doi.org/10.1063/5.0047571>

## I. INTRODUCTION

Today, much effort is focused on employing emerging materials and physical mechanisms for the purpose of data storage and computation.<sup>1–5</sup> Several schemes make use of Resistive Switching (RS), which refers to a large class of related phenomena wherein the resistance of a two-terminal device can be controlled via electrical stimuli.<sup>6</sup> These effects can be used, as in Resistive Random Access Memory (RRAM), to store bits as non-volatile resistance states. Resistive switches can be fabricated using a wide variety of CMOS-compatible materials<sup>7,8</sup> and are highly attractive due to their simple device structure, high speed, scalability,<sup>9</sup> and potential for 3D integration<sup>10</sup> as required by next generation memory and computing architectures.<sup>11</sup>

A central challenge for RRAM is the intrinsically stochastic nature of the RS process, which leads to large variability in the programmed resistance states and switching parameters.<sup>12,13</sup> Achieving an acceptable level of control over the switching process will require in-depth understanding of the statistical processes at play, as well as optimization of the active material together with the control circuitry. For this purpose, it is necessary to drive memory cells through

a statistically significant number of switching cycles and to rapidly test different materials and modes of operation on a wafer probing system.

RRAM is commonly benchmarked by direct application of square voltage pulse sequences, but one of the shortcomings of this approach is that only the resulting resistance states are typically recorded, while the dynamics of the conductance changes in the material are very often left unmeasured. Quasistatic  $I$ ,  $V$  loops are an alternative measurement where switching is induced by an applied voltage that is continuously ramped at a low speed ( $\sim 1$  V/s) between positive and negative values. The current resulting from these sweeps is sampled and plotted against the applied voltage, as shown in Fig. 1. Such  $I$ ,  $V$  loops are relatively rich in information, and important parameters such as the resistance non-linearity, voltage/current switching thresholds, and details of the transition behavior can be extracted. However, the low speed of the measurement puts excessive electrical stress on the device and makes experiments involving more than a few hundred switching cycles impractical.

While negative resistance transitions in RS materials can occur on timescales below 1 ns,<sup>14–16</sup> the nanoscale material volumes

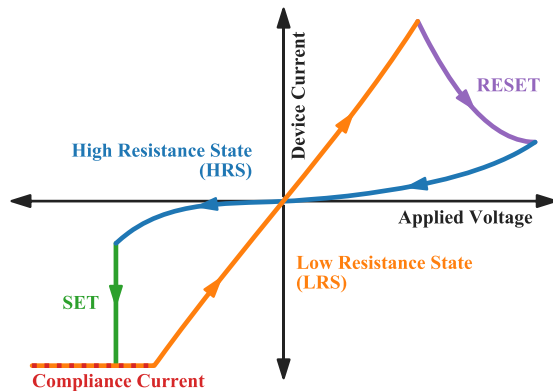


**FIG. 1.** Schematic diagram of a single RRAM  $I, V$  loop cycle from which important switching parameters can be extracted. Measurements of such loops show statistical variation of these parameters both device-to-device and cycle-to-cycle.

involved cannot normally survive prolonged exposure to the voltage required to initiate the transition, as the current density quickly reaches levels that cause irreversible thermal damage.<sup>17</sup> Thus,  $I, V$  loop measurements are only possible in the context of a feedback mechanism to prevent runaway destruction of the RS device. Externally implemented current limiting such as the current compliance function of commercial Source Measure Units (SMUs) and Semiconductor Parameter Analyzers (SPAs) is known to cause large overshoots that can lead to catastrophic damage to cells<sup>18,19</sup> (Fig. 2) and can otherwise strongly influence the measurements.<sup>20,21</sup> Patterning RS devices directly on MOS transistors provides superior current limiting, but the required integration limits the materials available and necessitates long fabrication cycle times.<sup>20,22,23</sup> A simpler approach from the point of view of fabrication is to integrate

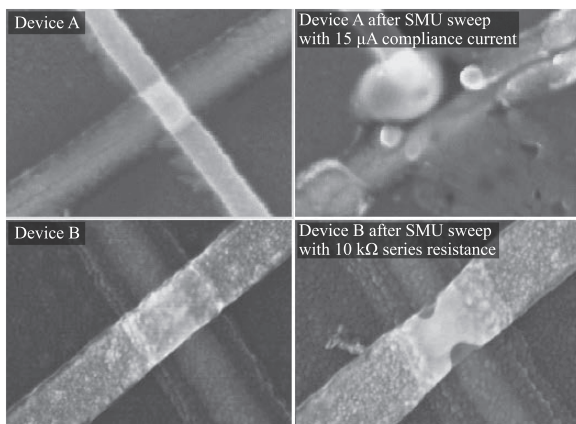


**FIG. 2.** Damage induced by current overshoots in 100 nm crossbar structures with 30 nm Pt top and bottom electrodes and a 100 nm VOx switching layer. Device A was subjected to a voltage sweep by an SMU with a 15  $\mu\text{A}$  current compliance setting. Device B, protected by a 10  $\text{k}\Omega$  external series resistor, was swept similarly, but was still damaged by the capacitive discharge of an interconnecting 20 cm coaxial cable. Although the cells are visibly destroyed, both, nevertheless, continued to show measurable RS behavior as a conducting path still existed through what remained of the oxide material.

fixed resistors in series with the devices.<sup>24,25</sup> However, the large linear feedback introduced by this relatively inflexible method significantly affects the switching behavior<sup>26,27</sup> and can push the operating voltage outside of the practical range.

The circuit design reported in this work represents a new way to characterize RS devices. It can be used to suppress current overshoots and collect very large volumes of  $I, V$  sweeping characteristics without the requirement of CMOS integration. We demonstrate collection of  $10^5$  switching cycles per second, which is highly useful for studying the stochastic nature of switching processes.

## II. EXTERNAL CURRENT LIMITING AMPLIFIER

### A. Design principles

For the purpose of rapidly testing devices with minimal nano-fabrication overhead, compatibility with isolated two-terminal structures is necessary and should be provided by an external Current Limiting Amplifier (CLA) circuit placed in series with the Device Under Test (DUT) in a setup similar to that shown in Fig. 3. When the series combination is driven by a voltage waveform, the circuit should provide a variable current limit in the approximate range 10  $\mu\text{A}$ –1 mA in the forward polarity (SET direction). Because of the self-limiting nature of the RESET process under voltage control, current should flow through the circuit unimpeded in the reverse polarity (RESET direction).

To avoid any influence of the circuit on the switching process before the current limit is reached, the circuit should present a negligible impedance for all currents below the limit. Only when the DUT current reaches the limit, the circuit should rapidly transition into a current source behavior to terminate the runaway switching process. In other words, the circuit should ideally present a frequency independent  $I, V$  characteristic, as shown in Fig. 4(a) in series with the

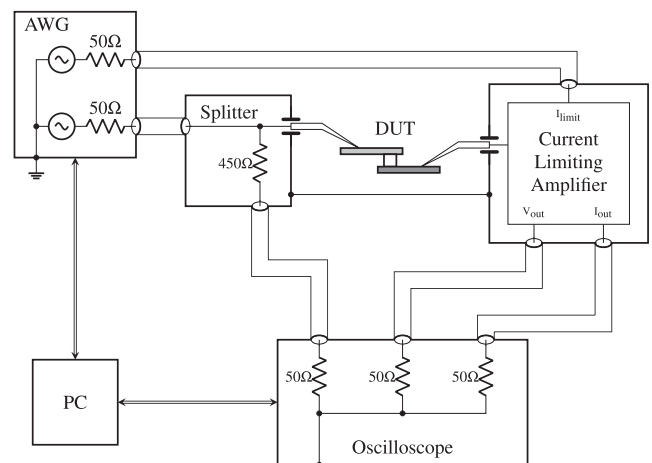


**FIG. 3.** Schematic of a measurement setup using the current limiting amplifier circuit. A two channel arbitrary waveform generator (AWG) applies a driving signal to the DUT as well as a signal to control the value of the forward current limit. An oscilloscope measures simultaneous samples of the voltage at both electrodes, as well as the device current. A jumper connects the ground planes of the left and right probes to reduce interference and inductance in the signal path.

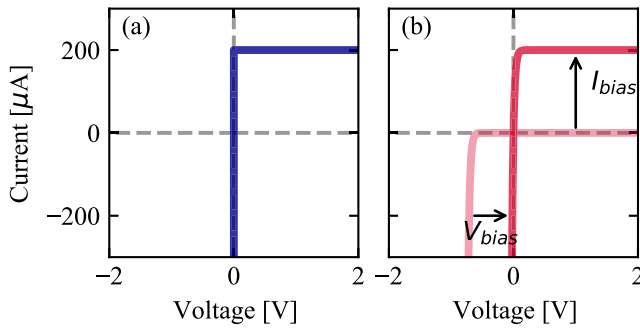


**FIG. 4.** The current limiting  $I, V$  characteristic intended to be placed in series with the DUT. In the ideal case (a), the differential resistance is zero below the adjustable current limit (here  $200 \mu\text{A}$ ) and is infinite above the adjustable current limit. An approximation (b) can be realized using a common-base amplifier with voltage and current bias.

device. The circuit should be highly stable for a variety of loads, and its design should be as simple as possible in order to easily distinguish the role of the DUT in measurements of the overall electrical response.

Crucially, any overshoot above the current limit following a SET transition should be suppressed as much as possible. Because such overshoots are caused by the stray capacitance at the terminal of the current limiting circuit, this capacitance is considered a critical design parameter to be minimized. It is therefore not an option to connect the CLA to the DUT over a length of coaxial cable, as this would present an effective capacitance of  $100 \text{ pF/m}$ . To reduce this capacitance, the probing circuit needs to be mounted as close as possible to the DUT, and a short unshielded probe needle should be mounted directly to its circuit board.

In this type of measurement setup, two important bandwidths can be distinguished: the first is the bandwidth of the application of voltage signals to the DUT, and the second is the bandwidth of the measurement of current through the DUT. Simplistic external current limiting approaches using a series resistor or a common-source FET have the side effect of forming a low pass filter that limits one of these bandwidths depending on which side of the DUT the current limiter is positioned. In such setups, the limited bandwidth also depends on the resistance state of the DUT and on the current limit used. These bandwidth limiting effects should be circumvented in the CLA design. For all current limit settings and DUT states, the bandwidth of voltage application should be limited only by the AWG ( $100 \text{ MHz}$ ) and the DUT parasitics. The bandwidth of the low-noise current measurement should be large enough to accommodate the detection of rapid switching events with a rise time below  $100 \text{ ns}$ .

## B. Implementation

The fundamental idea behind the presented circuit design is to use a single bipolar junction transistor (BJT)  $I, V$  characteristic to implement the desired current limiting response while also providing transimpedance amplification of the DUT current. Packaged discrete BJTs for radio frequency applications are available with very low parasitic capacitance, making them highly suitable here for use in the input stage. The common-base (CB) amplifier configuration is of particular interest as a high-bandwidth current buffer, featuring

a low input impedance and small feedback capacitance that does not suffer from the Miller effect. With voltage and current biasing, a CB amplifier can closely approximate the targeted current limiting  $I, V$  characteristic shown in Fig. 4. A simplified schematic of the input stage used to accomplish this is shown in Fig. 5.

The basic operation of this input stage is straightforward to analyze. Applying Kirchhoff's current law at the input node, it can be seen that whenever the DUT current  $I_d$  is less than the bias current  $I_{\text{bias}}$ , the BJT emitter current  $I_E$  is positive and the transistor will be in forward-active mode. In this mode, with an appropriate setting of  $V_{\text{bias}} \approx 0.7 \text{ V}$ , the input voltage  $V_{\text{in}}$  will be held close to  $0 \text{ V}$  due to the high forward transconductance of the BJT. Thus, for either positive or negative voltages applied to the DUT, the input stage effectively presents a low impedance to ground as long as  $I_d < I_{\text{bias}}$ . As  $I_d$  approaches  $I_{\text{bias}}$ , the BJT enters cut-off mode, where its effect on the circuit can be ignored and the input behaves as a current source with  $I_d = I_{\text{bias}}$ .

Ideally, the voltage bias  $V_{\text{bias}}$  should be chosen such that the input current is zero for an input voltage of zero (such that the curve of Fig. 4 intersects the origin). Considering an approximated Ebers–Moll model of the BJT, it follows that

$$V_{\text{bias}} = -nV_T \log\left(\frac{I_{\text{bias}}}{I_s} + 1\right), \quad (1)$$

where  $I_s$  is the saturation current of the base–emitter junction,  $V_T \approx 26 \text{ mV}$  is the thermal voltage, and  $n$  is the diode ideality factor. The output of this stage then gives an amplified voltage signal  $V_{\text{out}}$  that is linearly related to the input current

$$I_d = I_{\text{bias}} - \left(\frac{1 + \beta}{\beta}\right) \left(\frac{V_{\text{CC}} - V_{\text{out}}}{R_C}\right), \quad (2)$$

where  $\beta$  is the forward common-emitter current gain of the NPN transistor.

A full circuit diagram expanding on this concept is given in Fig. 6 with a prototype printed circuit board (PCB) layout also pictured in Fig. 7. Here,  $Q_1$  is the CB amplifier corresponding to that depicted in Fig. 5, and a nearly ideal voltage controlled current source is realized by the emitter degenerated cascade amplifier formed by  $Q_2$ ,  $Q_3$ , and  $R_2$ . The dependence of the current limit  $I_{\text{bias}}$  on the control voltage  $V_c$ , which is approximately linear for  $I_{\text{bias}} > 100 \mu\text{A}$ , is calibrated for  $V_c$  values between  $-10$  and  $-1 \text{ V}$  by

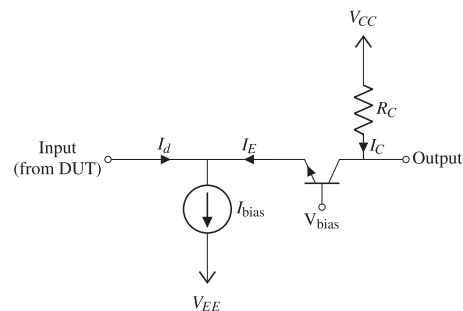


**FIG. 5.** A simplified diagram of a circuit implementing unipolar current limiting and transimpedance amplification. The value of the forward current limit is set by  $I_{\text{bias}}$ , and the input voltage is  $\sim 0 \text{ V}$  for input currents below this limit.

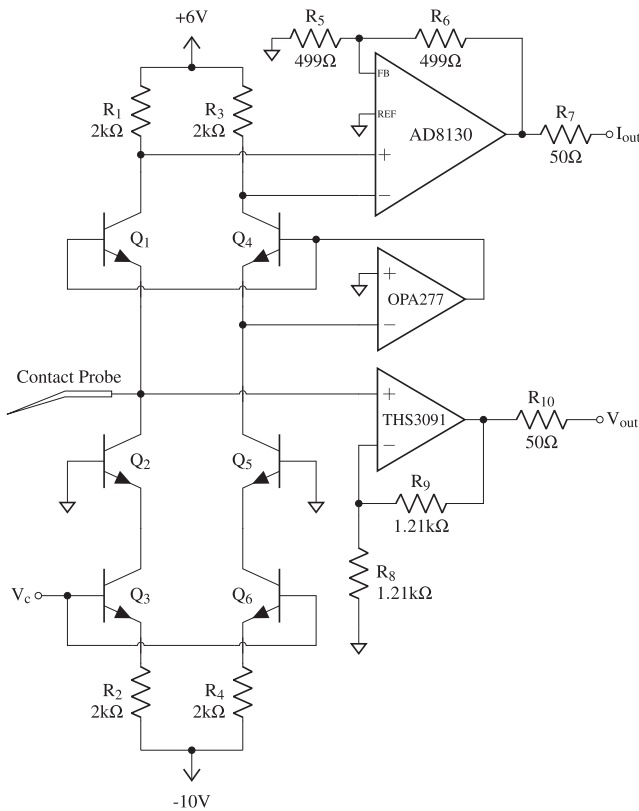


**FIG. 6.** Full schematic for the current limiting probing circuit. All BJT devices are ON Semiconductor part no. NSVF5501SKT3G. Transistors Q1–Q3 perform the current limiting function, with the current limit controlled by the input signal  $V_c$ . Regulated power supplies providing  $\pm 10$  and  $+6$  V are not shown.

an SMU measurement. The  $V_c$  signal is then generated according to the interpolation of the calibration table at the desired  $I_{bias}$  values.

Further circuitry in Fig. 6 is included to null voltage offsets and condition the output signals for transmission to 50  $\Omega$  oscilloscope inputs. From Eq. (1), it is seen that the ideal value of  $V_{bias}$  depends slightly on the value of  $I_{bias}$ . Therefore, simply using a constant value of  $V_{bias}$  would create offset voltages at the input terminal

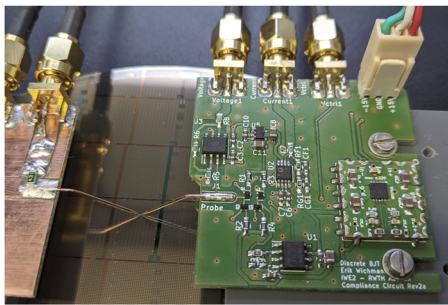


**FIG. 7.** Photograph of the probing circuit board contacting a prototype RRAM device. Left and right probes are mounted on independent micropositioners.

on the order of 10 – 100 mV as  $I_{bias}$  is varied. To automatically compensate this effect, a reference path  $R_3, Q_4, Q_5, Q_6$ , and  $R_4$  mirrors the components  $R_1, Q_1, Q_2, Q_3$ , and  $R_2$ , respectively, and is used to actively zero the input offset for all values of  $I_{bias}$  via OPA277. This same structure also generates a reference voltage for a differential measurement performed by AD8130, producing a low-offset output signal  $I_{out}$  proportional to the input current. A voltage follower (THS3091) with very low input capacitance (0.1 pF) is also placed directly at the input node, providing a simultaneous measurement of the DUT voltage drop.

### III. MEASUREMENT RESULTS

Current overshoots accompanying sudden negative resistance transitions are suppressed in our measurement scheme by minimizing the capacitance at the input node of the CLA. This is done by careful selection of the input transistors and by avoiding proximity of input traces to the ground plane. However, the parasitic capacitance cannot be fully eliminated, and the potential to create overshoots inevitably remains. Since overshoot transients tend to play a critical role in switching behavior in practice, it is important to characterize and model them.

In general, the time-dependent  $I, V$  trajectory of a current overshoot is not solely a characteristic of the measurement setup but is determined by the coupled dynamics of the DUT conductance and the driving circuitry. The duration and amplitude of the overshoot therefore depend on the type and history of the RS cell being measured and is not easily reproducible. To measure the overshoot characteristic in a standardized way, a test sample designed to imitate the resistive switching action was constructed using surface mount components. A mechanical reed relay in series with a 1.2 k $\Omega$  and in parallel with 100 k $\Omega$  was found to be well suited for this purpose, providing a controllable sub-nanosecond transition between two discrete resistance levels with negligible parasitic effects.

With the reed switch connected in the position of the DUT and biased by 1 V, the current transient following a resistance transition was measured with 350 MHz bandwidth (Fig. 8). Close agreement of the transient was found with the solution of a differential equation describing the charging of the CLA input node

$$C_p \frac{dV_d}{dt} = I_{bias} \left[ 1 - \exp\left(-\frac{V_d - V_a}{V_T}\right) \right] - \frac{V_d}{R_d}, \quad (3)$$

where  $C_p = 5.7$  pF is the parasitic capacitance at the input,  $V_d$  is the DUT voltage drop,  $V_a$  is the applied voltage, and  $R_d$  is the DUT resistance (here assumed to be a step function in time). Note that  $C_p$  includes the self-capacitance of the measured cell, which is  $\sim 0.5$  pF for the reed relay circuit. This should be taken into consideration in the memory cell design itself, where thin dielectric layers and large contact pads or device areas can contribute significantly to the total  $C_p$ , which intrinsically degrades the overshoot performance. Given the single parameter  $C_p$ , the simple model of Eq. (3) is expected to accurately characterize the transient response of the CLA circuit and should be incorporated with a physical device model to properly understand the complete picture of the coupled system during a measurement.

For comparison, the current overshoot transient induced using a modern SMU was measured under identical conditions. For the



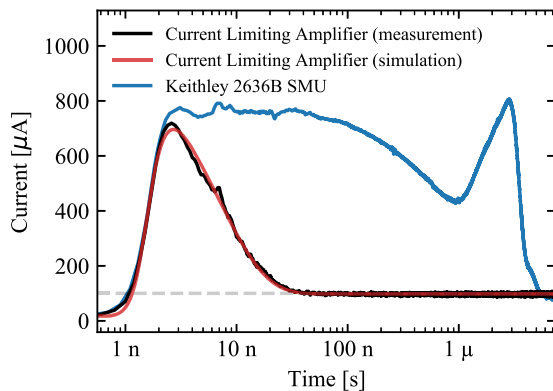


**FIG. 8.** Current overshoot characterization using a reed relay to abruptly switch from 100 to 1.2 k $\Omega$  at a time of 1 ns with 1 V applied and with a current limit of 100  $\mu$ A. Under these conditions, the CLA returned to the current limit in  $\sim$ 20 ns, whereas a commercial SMU produced a more complex overshoot response lasting several microseconds.

first 1  $\mu$ s after the resistance transition, the transient begins with the discharge of a 1 m coaxial cable, which was used to connect the instrument. Between 1 and 10  $\mu$ s, a proprietary feedback circuit is engaged and produces a long unpredictable current excursion before undershooting and eventually settling to the programmed current compliance level. Relative to this, the overshoot duration is reduced in the CLA measurement by over two orders of magnitude.

To demonstrate the RS cycling operation using the external CLA circuit, we tested a TaOx-based nano-scaled (100 nm) RRAM device. With the CLA input connected to the DUT top electrode, the current limit was set to 300  $\mu$ A and a triangular voltage signal with a period of 10  $\mu$ s and an amplitude of 1.5 V was applied to the DUT bottom electrode using a Rigol DG5102 AWG. The applied voltage and device current were sampled at 1.25 GS/s using a Picoscope 6404D deep-storage oscilloscope. In a single measurement lasting only one second,  $10^5$  full  $I$ ,  $V$  loops were successfully collected, each

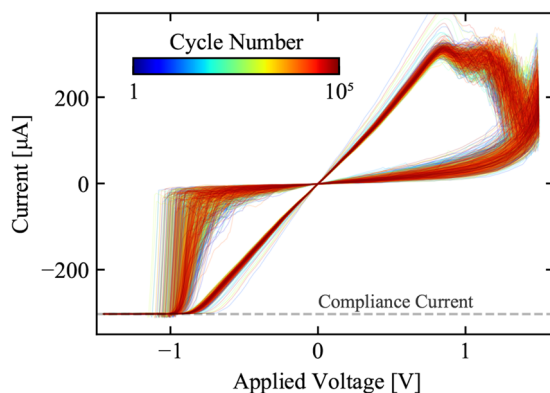


**FIG. 9.** A measurement of  $10^5$  consecutive  $I$ ,  $V$  loops collected in 1 s with the CLA circuit using a triangular voltage excitation and 300  $\mu$ A current limit. Data are smoothed by a 15 sample moving average, and every 100th cycle is plotted. To conform to plotting convention, the applied voltage is defined as the negative of the AWG voltage.

containing 1564 8-bit  $I$ ,  $V$  samples (Fig. 9). It is furthermore possible to collect millions of such cycles in a practical amount of time by collating multiple measurement shots, creating powerful datasets for statistical evaluation of RS devices.

#### IV. CONCLUSION

Resistive switching devices are promising building blocks for future memory and neuromorphic architectures, with a salient property of large cycle-to-cycle variability. Conventional laboratory measurements of these cells commonly represent very different conditions from integrated systems and often have unclear implications for device applications. In particular, current overshoots during run-away resistance transitions hinder the ability to control and characterize the switching process. In this work, an external current limiting amplifier was developed to reduce the overshoot effect and allow for measurements of full  $I$ ,  $V$  loops at  $\sim 10^6$  times faster rates than commercial SMUs. The minimal design with low transistor count is relatively robust against load-induced instability and has the important advantage that its response is accurately predictable using a few idealized component models.

#### DATA AVAILABILITY

The data that support the findings of this study are available from the corresponding author upon reasonable request.

#### REFERENCES

- <sup>1</sup>D. J. Wouters, R. Waser, and M. Wuttig, *Proc. IEEE* **103**, 1274 (2015).
- <sup>2</sup>S. Yu and P.-Y. Chen, *IEEE Solid-State Circuits Mag.* **8**, 43 (2016).
- <sup>3</sup>G. W. Burr, R. M. Shelby, A. Sebastian, S. Kim, S. Kim, S. Sidler, K. Virwani, M. Ishii, P. Narayanan, A. Fumarola, L. L. Sanches, I. Boybat, M. Le Gallo, K. Moon, J. Woo, H. Hwang, and Y. Leblebici, *Adv. Phys.: X* **2**, 89 (2017).
- <sup>4</sup>V. K. Sangwan and M. C. Hersam, *Nat. Nanotechnol.* **15**, 517 (2020).
- <sup>5</sup>W. Ma, P.-F. Chiu, W. H. Choi, M. Qin, D. Bedau, and M. Lueker-Boden, in *International Conference on Rebooting Computing* (IEEE, 2019), pp. 1–9.
- <sup>6</sup>D. Ielmini and R. Waser, *Resistive Switching* (John Wiley & Sons, 2015).
- <sup>7</sup>H. Akinaga and H. Shima, *Proc. IEEE* **98**, 2237 (2010).
- <sup>8</sup>Y. Chen, *IEEE Trans. Electron Devices* **67**, 1420 (2020).
- <sup>9</sup>C. Nail, G. Molas, P. Blaise, G. Piccolboni, B. Sklenard, C. Cagli, M. Bernard, A. Roule, M. Azzaz, E. Vianello, C. Carabasse, R. Berthier, D. Cooper, C. Pelissier, T. Magis, G. Ghibaudo, C. Vallee, D. Bedeau, O. Mosendz, B. De Salvo, and L. Perniola, in *IEDM* (IEEE, 2016), pp. 4.5.1–4.5.4.
- <sup>10</sup>H.-Y. Chen, S. Brivio, C.-C. Chang, J. Frascaroli, T.-H. Hou, B. Hudec, M. Liu, H. Lv, G. Molas, J. Sohn, S. Spiga, V. M. Teja, E. Vianello, and H.-S. P. Wong, *J. Electroceram.* **39**, 21 (2017).
- <sup>11</sup>H. Li, T. F. Wu, S. Mitra, and H.-S. P. Wong, *IEEE Trans. Circuits Syst. I* **64**, 2263 (2017).
- <sup>12</sup>A. Chen and M.-R. Lin, in *International Reliability Physics Symposium* (IEEE, Monterey, CA, 2011), pp. MY.7.1–MY.7.4.
- <sup>13</sup>A. Fantini, L. Goux, R. Degraeve, D. Wouters, N. Raghavan, G. Kar, A. Belmonte, Y.-Y. Chen, B. Govoreanu, and M. Jurczak, in *International Memory Workshop* (IEEE, 2013), pp. 30–33.
- <sup>14</sup>A. C. Torrezan, J. P. Strachan, G. Medeiros-Ribeiro, and R. S. Williams, *Nanotechnology* **22**, 485203 (2011).
- <sup>15</sup>S. Menzel, M. von Witzleben, V. Havel, and U. Böttger, *Faraday Discuss.* **213**, 197 (2019).
- <sup>16</sup>M. von Witzleben, T. Hennen, A. Kindsmüller, S. Menzel, R. Waser, and U. Böttger, *J. Appl. Phys.* **127**, 204501 (2020).
- <sup>17</sup>J. Meng, B. Zhao, Q. Xu, J. M. Goodwill, J. A. Bain, and M. Skowronski, *J. Appl. Phys.* **127**, 235107 (2020).

- <sup>18</sup>Y. M. Lu, M. Noman, W. Chen, P. A. Salvador, J. A. Bain, and M. Skowronski, *J. Phys. D: Appl. Phys.* **45**, 395101 (2012).
- <sup>19</sup>S. Tirano, L. Perniola, J. Buckley, J. Cluzel, V. Jousseau, C. Muller, D. Deleruyelle, B. De Salvo, and G. Reimbold, *Microelectron. Eng.* **88**, 1129 (2011).
- <sup>20</sup>K. Kinoshita, K. Tsunoda, Y. Sato, H. Noshiro, S. Yagaki, M. Aoki, and Y. Sugiyama, *Appl. Phys. Lett.* **93**, 033506 (2008).
- <sup>21</sup>S. Ambrogio, V. Milo, Z. Wang, S. Balatti, and D. Ielmini, *IEEE Electron Device Lett.* **37**, 1268 (2016).
- <sup>22</sup>F. Nardi, D. Ielmini, C. Cagli, S. Spiga, M. Fanciulli, L. Goux, and D. J. Wouters, *Solid-State Electron.* **58**, 42 (2011).
- <sup>23</sup>C. Nguyen, C. Cagli, E. Vianello, A. Persico, G. Molas, G. Reimbold, Q. Rafhay, and G. Ghibaudo, in *Integrated Reliability Workshop* (IEEE, 2015), pp. 17–20.
- <sup>24</sup>A. Fantini, D. J. Wouters, R. Degraeve, L. Goux, L. Pantisano, G. Kar, Y.-Y. Chen, B. Govoreanu, J. A. Kittl, and L. Altimime, in *International Memory Workshop* (IEEE, 2012), pp. 1–4.
- <sup>25</sup>Y.-S. Fan, L. Zhang, D. Crotti, T. Witters, M. Jurczak, and B. Govoreanu, *IEEE Electron Device Lett.* **36**, 1027 (2015).
- <sup>26</sup>A. Hardtdegen, C. La Torre, F. Cuppers, S. Menzel, R. Waser, and S. Hoffmann-Eifert, *IEEE Trans. Electron Devices* **65**, 3229 (2018).
- <sup>27</sup>M. B. Gonzalez, M. Maestro-Izquierdo, F. Jiménez-Molinos, J. B. Roldán, and F. Campabadal, *Appl. Phys. Lett.* **117**, 262902 (2020).